Modelling and Fabrication of Anti-Stiction Features for Electrostatically Actuated Microsystems

Gurpreet Singh Gill[1*], Michal Zawierta[1], Dhirendra Kumar Tripathi[1], Mariusz Martyniuk[1], K.K. M. B. Dilusha Silva[1], Gino Putrino[1], Adrian Keating[2], Lorenzo Faraone[1]

[1]Deaprtment of Electrical, Electronics and Computer Engineering, [2] Department of Mechanical Engineering; School of Engineering, The University of Western Australia, Perth, WA – 6009, Australia
* gurpreet.gill@research.uwa.edu.au

In electrostatically actuated microelectromechanical systems (MEMS), the risk of snapping-down moveable beams and membranes increases with decreasing gap between actuation electrodes. Van der Waals forces play a significant role in subsequent stiction of actuated beams with the substrate or other surfaces. In order to enable recovery of the MEMS devices from the snap-down position, the role of size and roughness of the contact surface between anti-stiction bumps and the underlying surface is studied. This paper examines the design parameters of anti-stiction bumps, which allow restoring forces to recover from snap-down position and avoid device failure. Subsequently, the fabrication of these bumps is presented.

1. Introduction

Microelectromechanical system (MEMS) technologies employing suspended cantilevers or membranes often use electrostatic actuation in order to induce mechanical motion [1]–[3]. These devices are generally fabricated as parallel plate capacitors formed between a fixed bottom electrode and a mechanically suspended electrode that is moving downward as a result of electrostatic attraction between the electrodes. The pull-in phenomena during electrostatic actuation limit the tunable range of these devices, leading to snap-down of moveable parts. Snap-down failure generally occurs when the suspended electrode moves more than one third of the initial electrode separation [3]. Snap-down is defined as the condition where the restoring spring force of the suspended structure is overwhelmed by the electrostatic attraction force towards the substrate. This restricts the operating range of the device and may lead to permanent deformation or failure.

Surface forces are of particular importance in MEMS because of the high surface to volume ratio of thin-films [4]. Consequently, surface forces, such as van der Waals forces, between two adhered layers can dominate over the mechanical restoration forces of the structure, which, in the event of snap-down, may lead to permanent failure of the device. The Van der Waals forces between two surfaces are proportional to the contact area. This contact area can be reduced by introducing so-called anti-stiction bumps. Their purpose is the reduction of the contact area which leads to a significant reduction of the Van der Waals forces during the contact event. These anti-stiction bumps also allow the possibility of recovery of the snapped-down MEMS devices provided that the structural restoration forces are sufficiently large. As such, the size of anti-stiction bumps and roughness of the contact area between bumps and substrate play a crucial role in eliminating the permanent snap-down failure event in MEMS devices, which is highly desirable for device long term reliability [5]. In this contribution, we present a brief overview of the theory of stiction, followed by theoretical evaluation of optimum size of the anti-stiction bumps and the role of surface roughness in overcoming Van der Waals attractive forces, aiming to enable structural recovery of suspended structures. We subsequently present anti-stiction bumps fabricated either as a part of the moveable suspended structure or in contact with the fixed substrate.

2. Theory and analysis of stiction

In electrostatically actuated MEMS devices, the electrostatic tuning of suspended layers is achieved by applying a voltage difference between moveable and fixed electrodes. The balance between electrostatic attraction force and the mechanical restoring force controls the extent of the tunable gap before uncontrolled pull-in occurs. Subsequently, the van der Waals forces can adhere the snapped down surface permanently to the substrate.

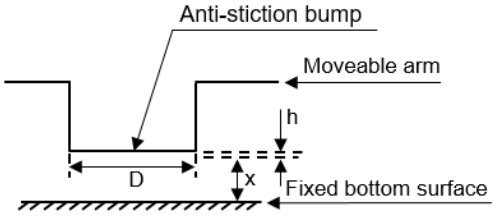

Figure 1: Cross-sectional view of a cylindrical anti-stiction bump incorporated within the suspended beam having diameter (D), roughness (h) at the bottom surface, and a gap (x) between the bottom surface of the anti-stiction bump and substrate/ fixed bottom electrode.

The theoretical model in this paper is based on the cross-sectional view of the anti-stiction bump shown in Figure 1. We consider a cylindrical anti-stiction bump geometry of depicted shape and size are fabricated within the actuating beam. As shown in Figure 1, D is the diameter of the bump and the total gap between the bump and substrate is equal to the sum of the suspended distance, x, and the effective contact roughness at the bottom surface of anti-stiction bump, h. The mechanical restoring force of structure can be expressed as:

$$F_{res} = -kx, \tag{1}$$

where k is the spring constant and x is the deflected distance of the suspended structure, as depicted in Figure 1.

When these two parallel surfaces come in to contact the van der Waals forces play a significant role can be expressed as [5]:

$$\mathrm{F_{vdW}} = -\frac{A}{6\pi h^3}\pi\left(\frac{D}{2}\right)^2, \tag{2}$$

where $A = k_b T_{room}$ is the haymaker constant, k_b is Boltzmann's constant, and T_{room} is the room temperature in Kelvin.

Under the influence of van der Waals forces for the recovery of a structure from collapsed state, the mechanical restoring force must be higher than the Van der Waals attraction force. Comparing Eqs 1 and 2 allow us to determine the spring constant of the structure that is required to recover a structure from snap-down state. This can be expressed as:

$$F_{res} > F_{vdW}, \tag{3}$$

$$kx > \frac{A}{6\pi h^3}\pi\left(\frac{D}{2}\right)^2, \tag{4}$$

Using Equation (4), we can estimate the spring constant required to recover an actuating structure from snap-down position using the structural restoration force. Minimising the area of contact between the two surfaces or increasing their effective contact roughness reduces the van der Waals force between the two surfaces aiding structural restoration.

We can analytically calculate the impact of contact surface area of anti-stiction bumps on the required spring constant. This is shown in Figure 2, where the calculated spring constant that is required to mechanically recover a snapped-down cylindrical bump is plotted as a function of the diameter of the anti-stiction bump for two different value of surface roughness, h. The first value for h was the universal roughness cut-off value of 0.165 nm, which is considered as the smoothest achievable surface for the anti-stiction bumps [5]. The second value for h was selected as 4.2 nm, which is the typical RMS value achieved by silicon nitride films deposited by Inductively Coupled Plasma Chemical Vapour Deposition (ICPCVD). In our calculations shown in Figure 2, we set gap, x equal to 1 µm. We can observe in Figure 2 that the value of spring constant required to restore a device increases rapidly as the diameter of the anti-stiction bump increases. This is because an increase in the contact area leads to an increase in the Van der Waals attraction between two surfaces. As a result, a greater restoring force is required to restore the beam from the snap-down state. For the universal contact surface roughness, $h_{universal}$, and a cylindrical bump diameter of 1 µm the value of the restoring spring constant required is

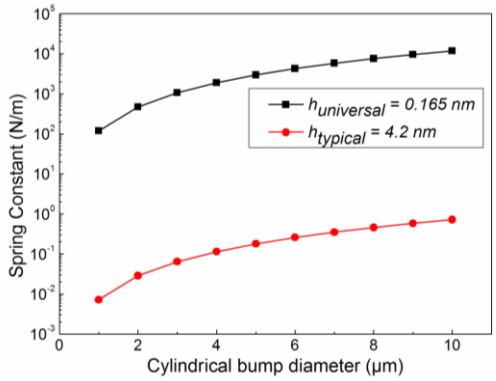

Figure 2: The spring constant required to mechanically recover a snapped-down cylindrical anti-stiction bump as a function of bump diameter for two different contact surface roughness values; $h_{universal} = 0.165\ nm$, that is generally considered as the smoothest achievable surface, and $h_{typical} = 4.2\ nm$, the typical RMS value achieved for silicon nitride films deposited using ICPCVD.

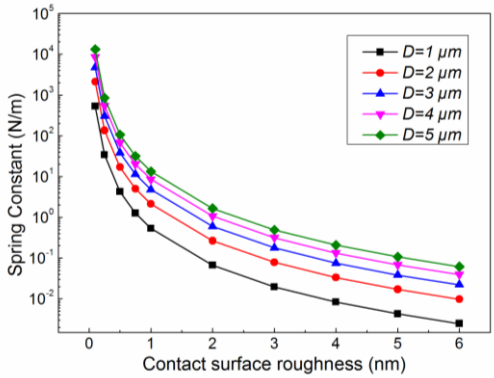

Figure 3: The spring constant required to mechanically recover a snapped-down cylindrical anti-stiction bump as a function of contact surface roughness calculated for anti-stiction bump diameters of 1 µm, 2 µm, 3 µm, 4 µm, and 5 µm.

1.18×10^2 N/m, which rises to 1.18×10^4 N/m for a 10 µm diameter. Similarly, for surfaces with an RMS roughness 4.2 nm (typically achievable in our laboratory) the value of spring constant increases from 7.16×10^{-3} N/m to 7.16×10^{-1} N/m with an increase in diameter from 1 µm to 10 µm.

The spring constant required to mechanically recover a snapped-down cylindrical anti-sticition bump as a function of contact surface roughness for a number of diameters is depicted in Figure 3. The displacement of the suspended structure, x was again set to 1 µm. It is evident from Figure 3 that an increase in contact surface roughness results in a significant decrease in the required restoring force represented here as the minimum required spring constant. These observation are common to all bump diameters considered in Figure 3.

3. Realisation of anti-stiction bumps

We have demonstrated two different types of anti-stiction bumps to protect MEMS structures from permanent snap-down failure. In the first type, the anti-stiction bumps were fabricated within the suspended beam using a conformal silicon nitride layer deposited by an Oxford Instruments Plasmalab80Plus ICPCVD. This silicon nitride

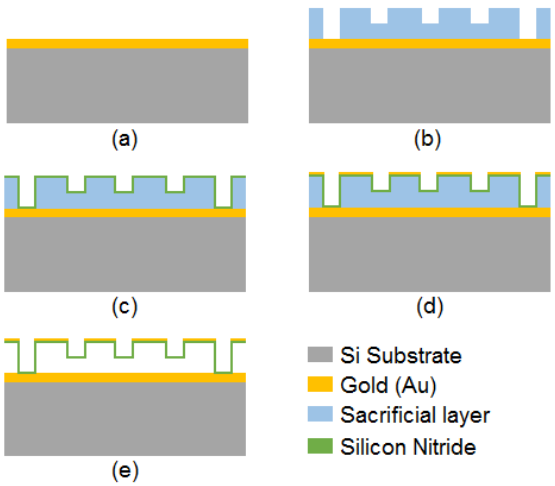

Figure 4: Fabrication process flow for the realisation of anti-stiction bumps within the suspended beam. (a) deposition of bottom metal (Au) electrode, (b) spinning of polyimide sacrificial layer and its patterning using photo-lithography (c) deposition of a conformal SiN_x ICPCVD layer, (d) deposition and patterning of the top metal (Au) electrode, and (e) removal of the sacrificial layer to release suspended structure.

layer was deposited over a pre-defined cylindrical geometry within the underlying sacrificial layer. The fabrication process flow of the anti-stiction bumps is presented in Figure 4.

Figure 5 shows the scanning electron microscope (SEM) image of the suspended anti-stiction bump fabricated within the actuation beam. This cross-section was fabricated with the help of focused ion beam (FIB) technique.

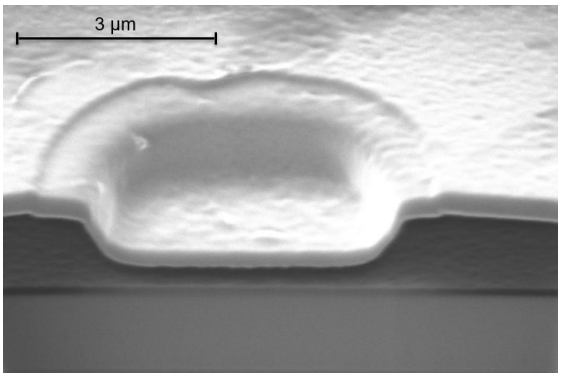

Figure 5: Cross-sectional scanning electron micro-graph of a suspended anti-stiction bump fabricated within the actuation beam.

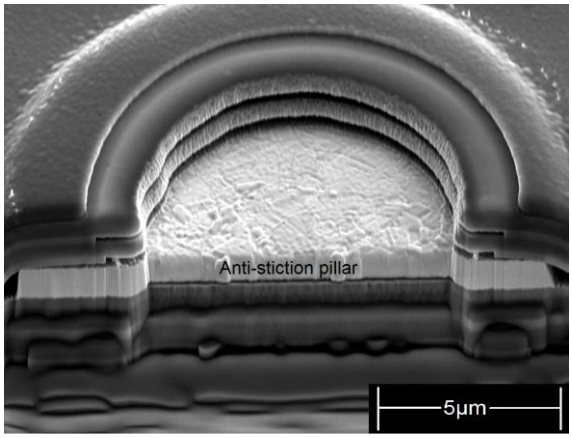

Figure 6: SEM cross-section of 16 µm metal pillar fabricated on the substrate. Image is taken while the anti-stiction bump is in contact with suspended membrane.

For another anti-stiction bump demonstration, rather than fabricating the anti-stiction bumps within the suspended structure, we focused on the fabrication of a fixed anti-stiction metal pillar, inside a Fabry-Perot cavity, formed between a bottom fixed, and a top suspended 5-layer Si/SiO_2 distributed Bragg reflectors (DBR). Figure 6 shows the anti-stiction pillars, which were realised on the bottom DBR and, are of 16 µm in diameter and 750 nm in thickness. They were aligned with 12 µm diameter release holes created within the top suspended DBR, and provided access for the subsequent removal of the underlying sacrificial layer to form an air cavity between the DBR layers. The adopted geometry alignment limited the contact area to the periphery of the pillars further minimising the van der Waals adhesion. Additionally, these metal pillars were used to block the undesired light transmission through the etch holes towards an underlying the detector not shown in Figure 6. The SEM pillar cross-section shown in Figure 6 was formed with the help of a FIB technique and image was taken while the anti-stiction bump is in contact with the suspended membrane. Our experiments show that square membranes up to an area 500 μm^2 could be actuated to snap-down, with subsequent recovery and without permanent failure.

4. Comparison with other anti-stiction bumps realisations in the literature

Our realisations of anti-stiction bumps can be compared to various other literature reports. Fan *et al.* modified their process to minimize the effect of friction to the substrate in electrostatic micro-motors [6], [7]. They introduced hemispherical bushing within a polysilicon layer suspended over thin insulating layers of oxide and nitride. Due to its hemispherical geometry it provided minimisation of the contact area, while aiding in achieving the desired electrical isolation. These bushings are considered as the first reported anti-stiction bumps in MEMS devices and are shown in Figure 7. In another approach, shown in Figure 8, F. Kozlowski *et al.* created water repellent fluorocarbon (FC) bumps to avoid post release stiction of the cantilever to the substrate [8]. These bumps were created after the removal of the sacrificial layer via directional deposition using suspended cantilevers as a shadow mask.

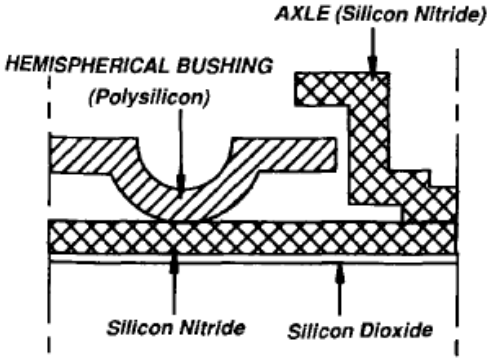

Figure 7: Hemispherical bushing within suspended polysilicon over an insulating layer of oxide and nitride provides a small contact area [6].

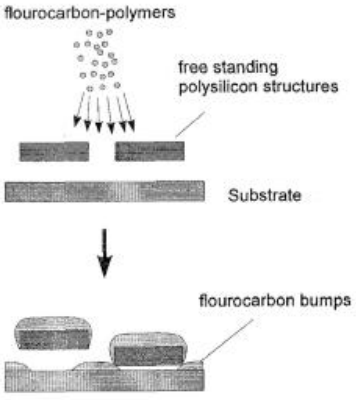

Figure 8: Anisotropic deposition of fluorocarbon (FC) bumps to protect the cantilever from stiction on the substrate [8].

In electrostatically driven MEMS speaker D. Tumpold *et al.* implemented a point array anti-stiction bumps on back-plate to eliminate stiction between the membrane and the back-plate, depicted in Figure 9 [9]. However, this realisation works well for these researcher, while another

group of researcher fabricated a similar fashioned point array bumps, which broke their cantilever structure because of its sharp tip [10]. M. Tuohiniemi *et al.* fabricated the anti-stiction bumps, shown in Figure 10 (right), by extending poly-Si/Air/poly-Si reflectors' inter-layer gap maintaining anchors in to Fabry-Perot cavity, shown in Figure 10 (left) [11]. Hence, these anti-stiction bumps eliminated the stiction issues in their Fabry-Perot interferometer, and simultaneously improved the Bragg reflector flatness.

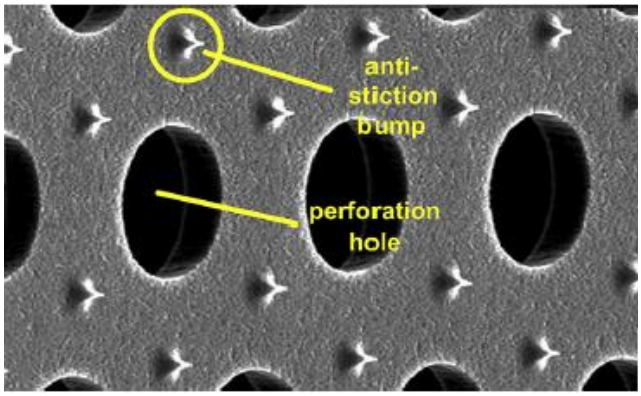

Figure 9: SEM image of point array anti-stiction bumps [9].

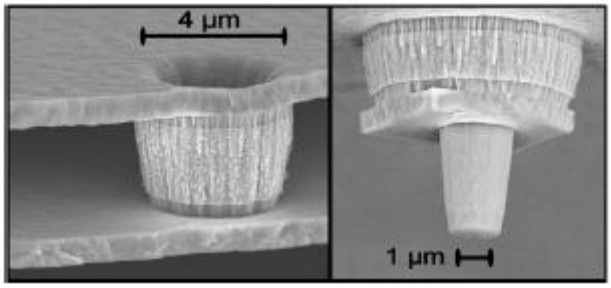

Figure 10: Anti-stiction bump (right) fabricated by extending the inter-layer gap maintaining anchor (left) into Fabry-Perot cavity [11].

5. Conclusion

The recovery of electrostatic devices from snap-down state with the help of mechanical restoring force depends directly on the minimization of Van der Waals forces between the two contacting surfaces. Considerations for the selection of the bump area, and roughness for the contact surface have been shown to lead a significant reduction in the attractive Van der Waals forces for minimization of the restoring forces required for recovery of snapped-down MEMS devices. Two complementary approaches for the fabrication of anti-stiction bumps were reported and compared to various realisations of anti-stiction bumps in the literature.

6. Acknowledgement

This work was performed at the Western Australian node of the Australian National Fabrication Facility (ANFF-WA), a company established under the National Collaborative Research Infrastructure Strategy to provide nano and micro-fabrication facilities for Australia's researchers. The authors thankfully acknowledge the facilities, and the scientific and technical assistance of the Centre for Microscopy, Characterisation & Analysis (CMCA), The University of Western Australia, a facility funded by the University, State and Commonwealth Governments, and The University of Western Australia for offering Scholarship for International Research Fees and Ad Hoc Postgraduate Scholarship.

7. References

[1] R. A. Coutu, P. J. Collins, E. A. Moore, D. Langley, M. E. Jussaume, and L. A. Starman, "Electrostatically tunable meta-atoms integrated with in situ fabricated MEMS cantilever beam arrays," *J. Microelectromechanical Syst.*, vol. 20, no. 6, pp. 1366–1371, 2011.

[2] X. Zhang, F. Y. Yamaner, and O. Oralkan, "Fabrication of Vacuum-Sealed Capacitive Micromachined Ultrasonic Transducers With Through-Glass-Via Interconnects Using Anodic Bonding," *J. Microelectromechanical Syst.*, vol. 26, no. 1, pp. 1–9, 2016.

[3] H. Mao *et al.*, "MEMS-Based Tunable Fabry-Perot Filters for Adaptive Multispectral Thermal Imaging," *J. Microelectromechanical Syst.*, vol. 25, no. 1, pp. 227–235, 2016.

[4] D. B. Heinz, V. A. Hong, C. H. Ahn, E. J. Ng, Y. Yang, and T. W. Kenny, "Experimental Investigation into Stiction Forces and Dynamic Mechanical Anti-Stiction Solutions in Ultra-Clean Encapsulated MEMS Devices," *J. Microelectromechanical Syst.*, vol. 25, no. 3, pp. 469–478, 2016.

[5] N. Tas, T. Sonnenberg, H. Jansen, R. Legtenberg, and M. Elwenspoek, "Stiction in surface micromachining," *J. Micromechanics Microengineering*, vol. 6, no. 4, pp. 385–397, 1996.

[6] L. S. Fan, Y. C. Tai, and R. S. Muller, "IC-processed electrostatic micromotors," *Sensors and Actuators*, vol. 20, no. 1–2, pp. 41–47, 1989.

[7] L. Fan, Y. Tai, and R. S. Muller, "IC-Processed Electrostatic Micro-motors," in *IEEE Int. Electron Devices Meeting*, 1988, pp. 666–669.

[8] F. Kozlowski, N. Lindmair, T. Scheiter, C. Hierold, and W. Lang, "A novel method to avoid sticking of surface-micromachined structures," *Sensors Actuators A Phys.*, vol. 54, no. 1–3, pp. 659–662, 1996.

[9] D. Tumpold, M. Stark, N. Euler-Rolle, M. Kaltenbacher, and S. Jakubek, "Linearizing an electrostatically driven MEMS speaker by applying pre-distortion," *Sensors Actuators, A Phys.*, vol. 236, pp. 289–298, 2015.

[10] S. L. Shi, D. P. Chen, Y. P. Jing, Y. Ou, T. C. Ye, and Q. X. Xu, "A novel method for sacrificial layer release in MEMS devices fabrication," *Chinese Phys. B*, vol. 19, no. 7, pp. 1–7, 2010.

[11] M. Tuohiniemi and M. Blomberg, "Surface-micromachined silicon air-gap Bragg reflector for thermal infrared," *J. Micromechanics Microengineering*, vol. 21, no. 075014, pp. 1–7, 2011.